

Journal of Materials Chemistry C

Accepted Manuscript



This is an *Accepted Manuscript*, which has been through the Royal Society of Chemistry peer review process and has been accepted for publication.

Accepted Manuscripts are published online shortly after acceptance, before technical editing, formatting and proof reading. Using this free service, authors can make their results available to the community, in citable form, before we publish the edited article. We will replace this *Accepted Manuscript* with the edited and formatted *Advance Article* as soon as it is available.

You can find more information about *Accepted Manuscripts* in the [Information for Authors](#).

Please note that technical editing may introduce minor changes to the text and/or graphics, which may alter content. The journal's standard [Terms & Conditions](#) and the [Ethical guidelines](#) still apply. In no event shall the Royal Society of Chemistry be held responsible for any errors or omissions in this *Accepted Manuscript* or any consequences arising from the use of any information it contains.

Facile synthesis of nanostructured carbon materials over Raney nickel catalyst films printed on Al₂O₃ and SiO₂ substrates

Jhieh-Fong Lin,^{a,b} Melinda Mohl,^a Mikko Nelo,^a Geza Toth,^a Ákos Kukovecz,^{c,d} Zoltán Kónya,^{c,e} Srividya Sridhar,^f Robert Vajtai,^f Pulickel M. Ajayan,^f Wei-Fang Su,^b Heli Jantunen^a and Krisztian Kordas^{a*}

^a Microelectronics and Materials Physics Laboratories, Department of Electrical Engineering, University of Oulu, Finland, P.O. Box 4500, FI-90570 Oulu, Finland

^b Department of Materials Science and Engineering, National Taiwan University, 1, Roosevelt Road, Section 4, Taipei 106-17, Taiwan

^c Department of Applied and Environmental Chemistry, University of Szeged, Rerrich Bela ter 1 H-6720 Szeged, Hungary

^d MTA-SZTE "Lendület" Porous Nanocomposites Research Group, Rerrich Bela ter 1 H-6720 Szeged, Hungary.

^e MTA-SZTE Reaction Kinetics and Surface Chemistry Research Group, Rerrich Bela ter 1, H-6720 Szeged, Hungary

^f Department of Material Science and NanoEngineering, Rice University, Houston, Texas 77005, United States.

Abstract

A quick and convenient approach which combines a printing process and chemical vapor deposition is developed for a facile construction of nanostructured metal-carbon composite structures. Films of porous Raney nickel catalyst particles are deposited on various substrates by stencil printing from dispersions of the catalyst and poly(methyl methacrylate) in 2-(2-butoxyethoxy)ethyl acetate. After removing the organic binders at elevated temperatures, the mesoporous Ni film is applied as a growth template for synthesizing nanostructured carbon materials on the surface. Depending on the synthesis conditions, carbon nanofibers and nanotubes as well as graphite deposits are found to form on the substrates allowing a robust and scalable production of carbon based inert electrodes of high specific surface area. Besides structural characterization of the composites by the means of scanning and transmission electron microscopy, Raman spectroscopy, X-ray diffraction, thermal gravimetric and surface adsorption analyses, the produced carbon/Raney nickel composites are also studied as electrodes in electrochemical capacitors (specific capacitance of $\sim 12 \text{ F}\cdot\text{g}^{-1}$) and in field emitter devices with low turn-on field ($< 1.0 \text{ V}/\mu\text{m}$). The results indicate the carbon/Raney nickel composites are suitable for direct integration on substrates used frequently in microelectronics.

Keywords: nanostructured metal-carbon composite, Raney nickel, stencil printing, chemical vapor deposition, electrochemical capacitor, field emitter

Introduction

In the past decades, carbon nanomaterials of different dimensionality such as fullerenes, carbon nanotubes and graphene have been widely studied and employed in various applications. These carbon materials with the sp^2 atomic-bonding structure own high specific surface area, superior electrical and mechanical properties as well as light weight making them truly multifunctional and particularly attractive for electrode applications. Since carbon nanotubes are typically synthesized on metal nanoparticles supported on oxides (typical diffusion barriers), direct applications of the nanotubes for electrodes requires a number of different subsequent steps including (i) functionalization and dispersion for inkjet printing conductive networks,^{1,2} (ii) sputtering with metals for soldering aligned films³ (iii) or dispersion and filtration for obtaining bucky papers.⁴ Another approach to achieve carbon nanotube based electrodes is a direct growth of the nanotubes on conductive surfaces such as aluminum,^{5,6} copper⁷ or Inconel super-alloys.⁸⁻¹¹ Lately, also three-dimensional porous networks of metal-carbon composites and hybrids have been proposed as potentially good candidates of electrodes in supercapacitors and field emitters.^{12,13}

Ni nanoparticles have been long used to grow carbon nanotubes and various other carbonaceous species. In fact Ni, as an excellent catalyst for hydrogenation/dehydrogenation of hydrocarbons is applied by the petrochemical and food industries for nearly 100 years. Since the first successful synthesis in 1924, Raney nickel has been widely applied because of its high specific surface area (can reach as high as $100 \text{ m}^2/\text{g}$) and good hydrogen storage ability. One major difficulty of the catalyst is its relatively easy deactivation caused by coking i.e. the formation of carbonaceous coating inhibiting the reactants to adsorb on the surface. The decomposition of acetylene on Raney nickel catalysts for instance can produce different kinds of carbonaceous materials such as filamentary or angular graphite laminae.¹⁴ Two important factors were suggested to influence the production of nanofilamentary carbons. One is the appearance of distorted nickel particles at elevated temperature due to the partial

melting of surficial nickel, while the other is associated with the local deposition of amorphous carbon to partially cover the catalyst. Such a partial poisoning of the catalyst (i.e. coking) results in location dependent decomposition of acetylene and consequently local temperature gradients, which has great importance in the localized dissolution and subsequent precipitation of carbon referred today as the vapor-liquid-solid growth model. Recent studies on the decomposition of methane over Ni nanoparticles and Raney-type catalyst also indicate the efficiency of methane decomposition correlate with the production of carbon nanofilaments.^{15, 16} A number of different studies revealed that the size of Ni particles has a decisive role in the type of carbon forming on the catalyst. Increasing catalyst size results in less efficient carbon diffusion through the catalyst giving rise to fiber formation instead of nanotubes (or in the extreme, poisoning the entire catalyst because of the growth of a carbon shell).^{17, 18} In this work, we explore further the possibility of applying Raney Ni catalyst to grow Ni/carbon composites by immobilizing the catalyst material on solid wafers such as polycrystalline alumina and oxidized Si. We show that stencil printing of the catalyst is a feasible route to fabricate mesoporous Raney nickel templates for subsequent growth of nanostructured carbons by chemical vapor deposition. The integrated, electrically conductive, three-dimensional Ni/carbon composites of high specific surface area on solid substrates are feasible for supercapacitor and field-emitter electrodes and can be attractive for further hybrid electronics especially for silicon on insulator (SOI) devices and for integrated microelectromechanical systems (MEMS).

Experimental

Preparation of Raney nickel paste and the stencil printing process

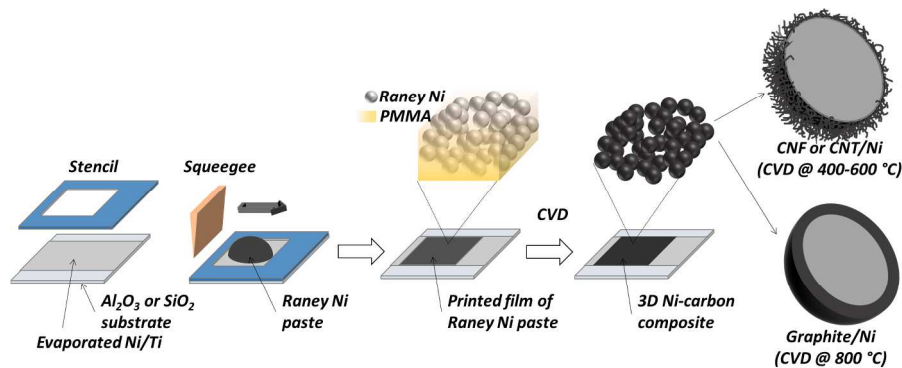
Raney® 2400 nickel (slurry in water), poly(methyl methacrylate) (PMMA, MW:350 g/mol), 2-(2-butoxyethoxy)ethyl acetate (C₁₀H₂₀O₄, >99.2%) were purchased from Sigma-Aldrich and used without further purification. To make catalyst paste for stencil printing, 88.0 g Raney nickel 2400 slurry is blend with 12.0 g poly(methyl methacrylate (PMMA) in 100.0 g 2-(2-butoxyethoxy)ethyl acetate (>99.2%) and then mixed in ball-mill for overnight. After the milling process, small aliquots of acetone are used to transfer the paste from the ball-mill to a beaker. To remove acetone from the paste, the container is heated to 90°C for about 15 minutes. The ready paste shows a typical non-Newtonian pseudoplastic fluid behavior with decreasing viscosity down to ~1.2 Pa·s as the shear rate is increased (Fig. S1).

In stencil printing process, we apply a laser cut stainless steel mask (thickness of 100 μm) having square shaped patterns of 15×15 mm² size through which the paste is doctored with a lateral blade movement rate of ~1.0 m/s. Wafers of Si with 200 nm SiO₂ layer (Si-Mat silicon materials) and polycrystalline alumina (thickness of 0.25 mm, Laser Tech Services) were used as substrates. Before the stencil printing, thin films of titanium (40 nm) and nickel (100 nm) were deposited on the substrate by e-beam evaporation and magnetron sputtering respectively, to ensure better adhesion of the catalyst and to help easy electrical interfacing of the grown structures in subsequent experiments. After the stencil printing process, the samples were annealed in a box furnace at 120°C in ambient condition for 15 minutes to remove the excess organic solvent (Scheme 1).

Synthesis of Ni-carbon composites

To grow CNTs and other carbonaceous materials, the patterned substrates were placed on a 2 inch size graphite heater in a cold-wall CVD reactor (Aixtron, Black Magic, UK). The samples were heated to

the desired synthesis temperature (400, 600 or 800°C with a heating rate 100°C·min⁻¹) in 500 sccm argon and 50 sccm hydrogen (5 mbar) and kept there for 30 minutes to facilitate the reduction of the catalyst. After this step, acetylene was introduced (flow rate of 10 sccm, at ~14 mbar) for a 20 min period to grow carbon and then the samples were cooled in a flow of argon (500 sccm) and hydrogen (50 sccm) (Scheme 1).



Scheme 1 Schematic drawing of the fabrication process including evaporation of under-metallization, stencil printing the catalyst and subsequent chemical vapor deposition of nanostructured carbons.

Characterization

Powder X-ray diffraction (XRD) pattern of carbon/catalyst composites were characterized by Bruker D8 Discovery XRD system with Cu K α radiation ($\lambda=1.5418$ Å). The patterns were recorded in the scan range of $2\theta=20-90^\circ$ with a step size of 0.025° and a scan step of 4 sec. To determine the quality of the synthesized carbon materials on catalyst surface Raman spectra of the products were assessed by a Horiba Jobin-Yvon Labram HR800 UV-vis μ -Raman instrument at $\lambda=488$ nm excitation. To confirm the production yield of carbon on the nickel catalyst under different growth processes, the carbon/nickel composite products were collected from the substrate and characterized by thermal gravimetric analysis (TGA, Setaram Labsys) in air with a heating rate of 5°C·min⁻¹ from room temperature to 1000°C.

In the course of the surface adsorption analysis, the composites were preheated to 200°C for 1 hour to desorb moisture followed by nitrogen adsorption-desorption in a volumetric adsorption analyzer (Quantachrome Nova 3000E). The specific surface area was calculated by the multipoint BET equation and the pore volume was acquired from the adsorption curve at 0.96 relative pressure (calculation using software Quantachrome NovaWin). Morphology and microstructure of the synthesized materials are studied by the means of transmission (TEM, Leo 912 Omega) and field emission scanning electron microscopy (FESEM, Zeiss Ultra Plus).

Electrochemical capacitors were constructed from pairs of similar mesoporous composites as electrodes being separated by 2 layers of filter papers (Whatman 1, Cat No 1001-047) as spacers. The mixture of aqueous solution of KOH (6M) and isopropyl alcohol with volume ratio 4:1 was applied as electrolyte. Isopropyl alcohol was added to improve the wetting of carbonaceous mesoporous electrode. The stack of electrodes and separator were mechanically clamped with a crocodile clip while performing cyclic voltammetry measurements (Princeton Applied Research VersaSTAT 3 potentiostat, voltage sweep rates of 0.05, 0.1, 0.25, and 0.5 V/s)

Results and discussion

Structure of the Raney nickel-carbon nanocomposites

After the growth processes at 400°C, 600°C, 800°C, and 1000°C, we observe various kinds of carbonaceous features forming nanostructured composites with the Raney catalyst (Figure 1 and Figure S2). Upon growth at 400°C or 600°C, carbon filaments appear on the surface of Raney nickel catalysts. Synthesis at 800°C results in much less filamentous products than seen at lower temperatures. TEM analysis reveals the filaments are mostly multi-walled carbon nanotubes in these samples (Fig. 2). Besides nanotubes, graphitic deposits of 40-50 nm thickness are found on the catalyst for the 800°C

growth. Experiments carried out at 1000°C made the porous catalyst structure to collapse (Figure S2) thus further experiments were not conducted.

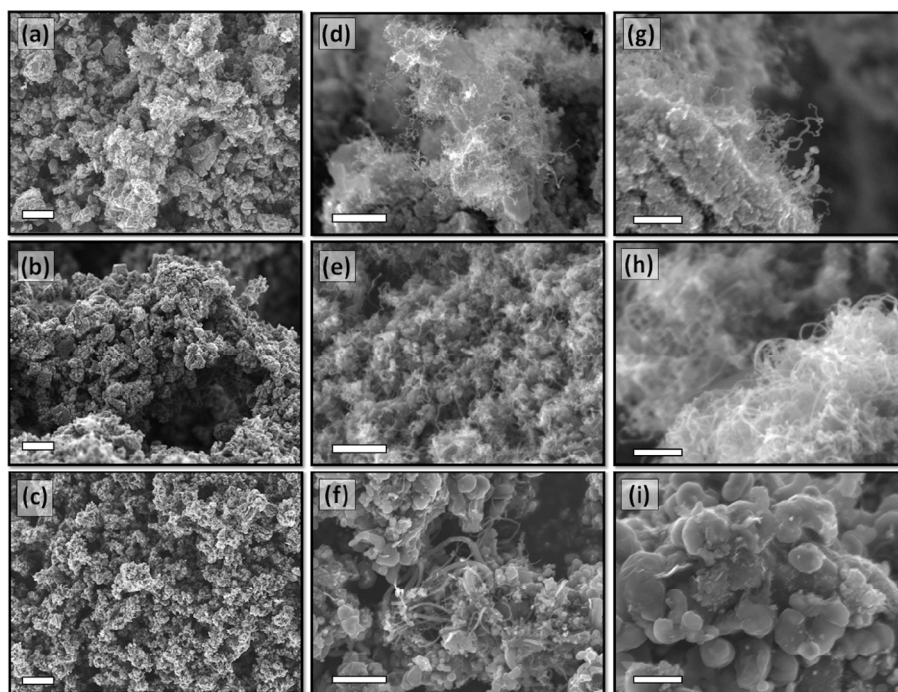


Figure 1 SEM images of porous structure of carbon growth on nickel mesoporous layer at (a, d, g) 400°C, (b, e, h) 600°C, (c, f, i) 800°C, the scale bar of (a-c), (d-f) and (g-i) are 10 μm , 1 μm and 400 nm, respectively.

As typically referred in the vapor-liquid-solid (VLS) growth model for carbon nanotubes on metal catalyst, the dissociation of hydrocarbon molecules (to carbon atoms and clusters) is the first main step. It is a thermally activated process proceeding in the gas phase but can be also catalyzed by the surface. After decomposition, the produced carbon species are adsorbed on and dissolved in the catalyst particle. Since the solubility of carbon in the metals highly depends on the surface curvature as well as on the temperature, minute fluctuations in such parameters can drive the carbon to phase separate (i.e. precipitate) and form carbonaceous deposits on the surface.¹⁹ The process is highly influenced by the diffusion rate of carbon inside the catalyst (bulk diffusion model) or on the surface of the metal

(surface diffusion model).^{20, 21} Based on the VLS model, we should observe rapid growth of CNTs at 800°C due to the faster rate of hydrocarbon decomposition and enhanced carbon diffusion in the catalyst, however the appearance of thick graphitic coating on the metal surface suggests a partial collapse of the mesoporous Ni structure, which is not favored to grow fibrous products. The massive precipitation of graphitic carbon layer on the surface is encapsulating the catalyst within a short period of time thus blocking the surface.

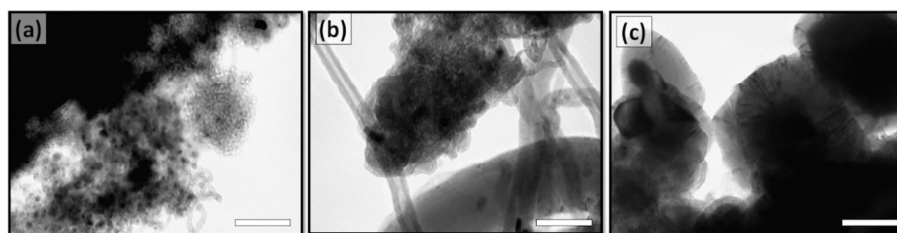


Figure 2 TEM images of carbon structure on nickel mesoporous layer after (a) 400°C, (b) 600°C, and (c) 800°C growth. The scale bars show 50 nm.

X-ray powder diffraction measurements of the synthesized carbon/Raney nickel composites (Fig. 3a) show reflections around 44.2° and 51.5°, which correspond to (111) and (200) planes of face-centered cubic nickel, respectively. Peaks that could be assigned to nickel oxide are not observed in the diffraction patterns. The decreased peak broadening with temperature (Table 1) indicates a partial sintering of the metal, which supports our earlier explanation on the limited filament growth at 800°C. The diffraction peak around 25.9° is due to the graphitic (002) planes being relatively intensive for the samples made at 600°C (carbon nanotubes) and 800°C (mainly graphite) as compared to those synthesized at 400°C. Raman spectroscopy analyses of the samples (Fig. 3b) are in agreement with the XRD results. The ratio of the G and D band peak intensities (i.e. sp^2 graphitic ordering around 1580 cm^{-1} vs. sp^3 hybridized carbons or defects at around 1355 cm^{-1}) is increasing significantly from 1.0 to 3.4 for the materials grown at 400°C and 800°C, respectively.

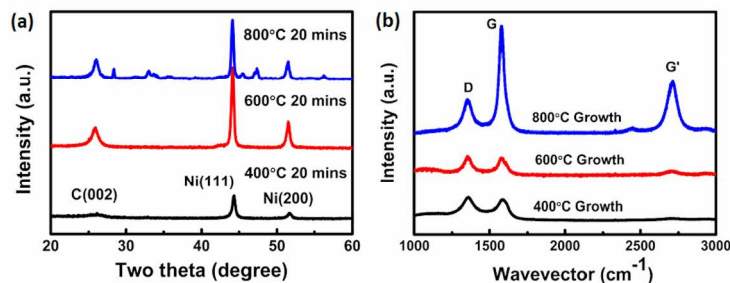


Figure 3 (a) X-ray diffraction patterns and (b) Raman spectra for carbon on Raney nickel nanostructured composites.

Table 1 Summary of crystal properties and Raman spectra of different carbon/nickel composites

Growth temperature (°C)	Crystal size by Ni (111) (nm)	Crystal size by Ni (200) (nm)	Raman I_G/I_D
400	21.5	15.8	1.0
600	23.7	19.6	1.0
800	27.4	25.9	3.4

To further evaluate the production yield of carbon materials after the different growth temperatures, we employed thermogravimetric analysis (from 300°C to 800°C in air) to assess the mass fraction of synthesized carbon in the composites. The weight loss of 29.0%, 48.0% and 36.0% for the samples grown at 400°C, 600°C and 800°C, respectively, indicates the optimum temperature for carbon growth is at 600°C in good accordance with the electron microscopy results shown earlier. On the other hand, it is worth mentioning that the degradation temperature increases with the growth temperature of the composites. Such improvement is because of the better crystallinity of carbon in the structures grown at elevated temperatures – in good agreement with our Raman and XRD results.

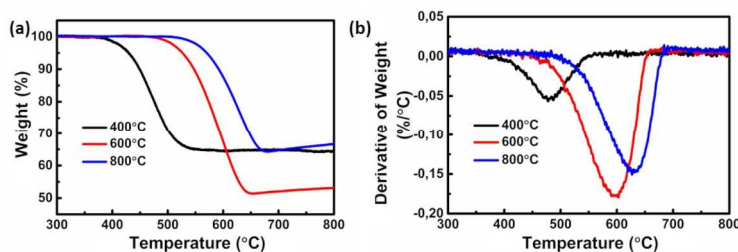


Figure 4 (a) Weight and (b) differential thermal gravimetric curves for different nanostructured Ni-carbon composites.

Although electron microscopy and X-ray diffraction analyses suggested a gradual sintering of the catalyst at elevated temperatures, it is not clear how much the porous nature of the originally highly nanostructured catalyst is kept for the nickel-carbon composites. In order to assess any changes in the porosity and surface area, the synthesized samples were subjected to surface adsorption analysis. According to the measurements, the specific surface area of Raney nickel ($100 \text{ m}^2/\text{g}$) is decreased to approximately 65, 36 and $15 \text{ m}^2/\text{g}$ after carbon growth in 400°C , 600°C and 800°C , respectively. On the other hand, the pore volume of the composites also decreases from 0.134 to 0.690 and 0.045 mL/g with increasing temperature (Fig. S3).

Raney nickel-carbon nanocomposites as electrode materials

The porous structure with high carbon content and the presumably good electrical conductivity of the nickel-carbon nanocomposites - which are in addition immobilized on solid surfaces - suggest applications of these materials for electrodes in supercapacitors and field emitters.

Cyclic voltammetry analysis (Fig. 5 and Table 2) of similar composite films in aqueous KOH electrolytes separated by cellulose membranes show rectangular CV curves with large hysteresis loops within a large voltage scan rate range (from 0.05 to $0.5 \text{ V}\cdot\text{s}^{-1}$) indicating the ideal capacitor behavior of

the stacks. By dividing the saturation current density from the voltage-current curve with the voltage scan rate ($0.25 \text{ V}\cdot\text{s}^{-1}$) and the weight of electrodes, the specific capacitance of the composites are $12.3 \text{ F}\cdot\text{g}^{-1}$, $2.5 \text{ F}\cdot\text{g}^{-1}$ and $1.0 \text{ F}\cdot\text{g}^{-1}$ (400°C , 600°C and 800°C growth, respectively). Although the obtained specific capacitance values are not very high, the value measured for the sample grown at 400°C is comparable with those reported for multi-walled carbon nanotubes ($18 \text{ F}\cdot\text{g}^{-1}$)⁸ and ($10\text{-}29 \text{ F}\cdot\text{g}^{-1}$)¹⁰ grown at 770°C from ferrocene/xylene precursors. Both the decreased specific surface area and pore size of these electrodes explain well the lowered capacitance with the increasing growth temperature (Table 2).

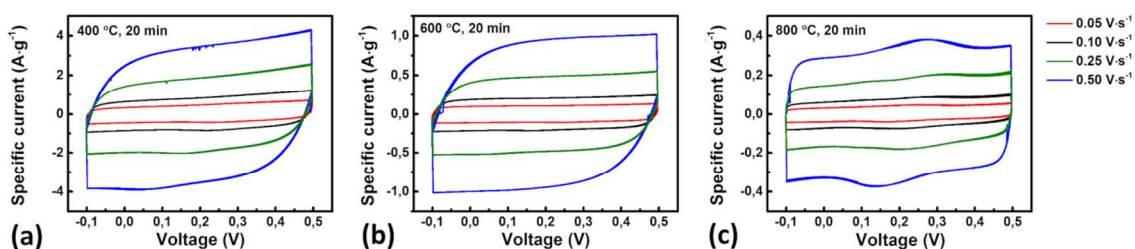


Figure 5 Cyclic voltammetry curves with different charge/discharge rates of carbon grown on nickel mesoporous layer after (a) 400°C , (b) 600°C , and (c) 800°C growth process.

Table 2 Properties of carbon structure on Raney nickel mesoporous layer

Growth temperature ($^\circ\text{C}$)	Specific surface area ($\text{m}^2 \text{ g}^{-1}$)	Pore volume ($\text{cm}^3 \text{ g}^{-1}$)	Carbon content (%)	Specific capacitance ($\text{F}\cdot\text{g}^{-1}$)
400	65.30	1.34×10^{-1}	29	12.3
600	35.90	6.90×10^{-2}	48	2.5
800	14.64	4.48×10^{-2}	36	1.0

Furthermore, these carbon/Raney nickel composite electrodes are also studied for cold cathode for field emission. As shown in Fig. 6, the turn-on voltage (which is the field required to give a current density of $10 \mu\text{A}/\text{cm}^2$) of three different electrodes are all below $0.9 \text{ V}/\mu\text{m}$, which is comparable with those

measured for carbon nanobuds ($0.65 \text{ V}/\mu\text{m}$)²² or for vertically aligned carbon nanotube arrays grown on Inconel ($1.5 \text{ V}/\mu\text{m}$ ¹¹ and $1.2 \text{ V}/\mu\text{m}$ ²³) or on Si ($0.8 \text{ V}/\mu\text{m}$ ²²) and significantly lower than that reported for screen printed carbon nanotubes ($3 \text{ V}/\mu\text{m}$ ²⁴).

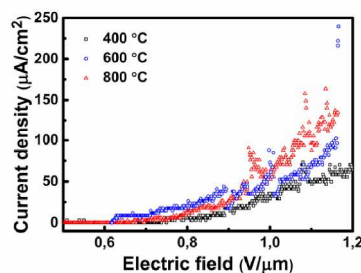


Figure 6 Field emission of carbon/Raney nickel composites.

The carbon nanostructures we obtained on stencil printed Ni catalyst hold promise for integrated field emitters that - in principle - could be patterned with a print resolution of a few tens of micrometers after some optimization of the paste (adding surfactants and/or decreasing particle size)²⁵ as well as selecting other potentially feasible printing processes such as screen,²⁶ gravure²⁷ or inkjet²⁸ instead of stencil printing. The method we described in this report may be optimized even further to allow entirely roll-to-roll compatible fabrication without the need for using vacuum processes. For instance, instead of the evaporated adhesion promoting under-metallization layers, one could apply thick-film printed conducting pastes consisting of some glass frit (binder between metal layer and substrate) before applying the Raney Ni pastes. Another approach could be a direct mixing of the glass frit into the Raney Ni paste along with organic dispersants so that the catalyst is immobilized with enhanced adhesion on the substrate in a single deposition step.^{29,30}

Conclusions

In summary, we developed a facile fabrication process for porous nanostructured metal-carbon composites by the combination of stencil printing and chemical vapor deposition processes. Patterns of catalyst films for subsequent growth of carbon nanomaterials (nanotubes, fibers and few layer graphite coatings) were obtained by stencil printing a Raney nickel based paste on alumina and SiO₂ substrates. The morphology of deposited carbon materials could be adjusted from nanofiber to nanotube and graphitic carbon layers by simply tuning the growth temperature. The nanostructured and porous carbon/nickel composites were found suitable for integrated electrochemical double-layer capacitor with specific capacitance up to 12.3 F·g⁻¹) as well as for cold cathode field emission electrodes with turn-on field lower than 0.9 V/μm. Since stencil printing is a cost-effective and relatively simple method for depositing microscopic patterns of a number of different nanomaterials besides the demonstrated Ni catalyst, we consider the results reported here may be implemented and optimized further to fabricate supercapacitor and field emitter electrodes as well as other components for applications in microelectronics even in bulk quantities.

Acknowledgements

We thank Elina Jansson (VTT Technical Research Centre of Finland) for her help in viscosity measurements. The financial support of the M-ERA.NET (VOCSSENSOR, OTKA, NN 110676), Academy of Finland (Suplacat and Optifu) and EU FP7 (Susfoflex, 289829 and Hippocamp, 608800) projects are acknowledged.

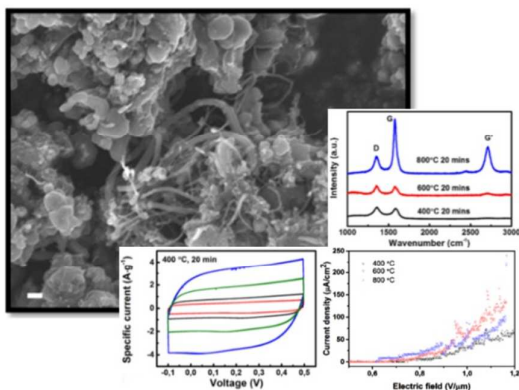
References

1. K. Kordas, T. Mustonen, G. Toth, H. Jantunen, M. Lajunen, C. Soldano, S. Talapatra, S Kar, R. Vajtai, P. M. Ajayan, *Small*, 2006, **2**, 1021.
2. E. Gracia-Espino, G. Sala, F. Pino, N. Halonen, J. Luomahaara, J. Maklin, G. Toth, K. Kordas, H. Jantunen, M. Terrones, P. Helisto, H. Seppa, P. M. Ajayan, R. Vajtai, *ACS Nano*, 2010, **4**, 3318.
3. G. Toth, J. Maklin, N. Halonen, J. Palosaari, J. Juuti, H. Jantunen, K. Kordas, W. G. Sawyer, R. Vajtai, P. M. Ajayan, *Adv. Mater.*, 2009, **21**, 2054.
4. M. Kaempgen, M. Lebert, N. Nicoloso, S. Roth, *Appl. Phys. Lett.* 2008, **92**, 094103.
5. R. Ummethala, V. O. Khavrus, A. Leonhardt, B. Buchner, J. Eckert, *Chem. Vap. Deposition*, 2012, **18**, 326.
6. C. Emmenegger, P. Mauron, A. Zuttel, C. Nutzenadel, A. Schneuwly, R. Gallay, L. Schlapbach, *Appl. Surf. Sci.*, 2000, **162**, 452.
7. G. Atthipalli, Y. Tang, A. Star, J. L. Gray, *Thin Solid Films*, 2011, **520**, 1651.
8. S. Talapatra, S. Kar, S. K. Pal, R. Vajtai, L. Ci, P. Victor, M. M. Shaijumon, S. Kaur, O. Nalamasu, P. M. Ajayan, *Nat. Nanotechnol.*, 2006, **1**, 112.
9. K. Aitola, J. Halme, N. Halonen, A. Kaskela, M. Toivola, A. G. Nasibulin, K. Kordas, G. Toth, E. I. Kauppinen, P. D. Lund, *Thin Solid Films*, 2011, **519**, 8125.
10. N. Halonen, J. Maklin, A. R. Rautio, J. Kukkola, A. Uusimaki, G. Toth, L. M. Reddy, R. Vajtai, P. M. Ajayan, K. Kordas, *Chem. Phys. Lett.*, 2013, **583**, 87.
11. S Sridhar, L. Ge, C. S. Tiwary, A. C. Hart, S. Ozden, K. Kalaga, S. Lei, S. V. Sridhar, R. K. Sinha, H. Harsh, K. Kordas, P. M. Ajayan, R. Vajtai, *ACS Appl. Mater. Interf.*, 2014, **6**, 1986.
12. Z. Yan, L. L. Ma, Y. Zhu, I. Lahiri, M. G. Hahm, Z. Liu, S. B. Yang, C. S. Xiang, W. Lu, Z. W. Peng, Z. Z. Sun, C. Kittrell, J. Lou, W. B. Choi, P. M. Ajayan, J. M. Tour, *ACS Nano*, 2013, **7**, 58.

13. Z. J. Fan, J. Yan, L. J. Zhi, Q. Zhang, T. Wei, J. Feng, M. L. Zhang, W. Z. Qian, F. Wei, *Adv. Mater.*, 2010, **22**, 3723.
14. R. T. K. Baker, M. A. Barber, P. S. Harris, F. S. Feates, R. J. Waite, *J. Catal.*, 1972, **26**, 51.
15. N. Mahata, A. F. Cunha, J. J. M. Orfao, J. L. Figueiredo, *Appl. Catal. A*, 2008, **351**, 204.
16. A. F. Cunha, J. J. M. Orfao, J. L. Figueiredo, *Appl. Catal. A*, 2008, **348**, 103.
17. H. Y. Wang, A. C. Lua, *J. Phys. Chem. C*, 2012, **116**, 26765.
18. M. Chhowalla, K. B. K. Teo, C. Ducati, N. L. Rupesinghe, G. A. J. Amaratunga, A. C. Ferrari, D. Roy, J. Robertson, W. I. Milne, *J. Appl. Phys.*, 2001, **90**, 5308.
19. N. Halonen, K. Kordas, G. Toth, T. Mustonen, J. Maklin, J. Vahakangas, P. M. Ajayan, R. Vajtai, *J. Phys. Chem. C*, 2008, **112**, 6723.
20. S. Hofmann, C. Ducati, J. Robertson, B. Kleinsorge, *Appl. Phys. Lett.*, 2003, **83**, 135.
21. O. Pitkanen, N. Halonen, A.-R. Leino, J. Maklin, A. Dombovari, J.-F. Lin, G. Toth, K. Kordas, *Top. Catal.*, 2013, **56**, 522.
22. A. G. Nasibulin, P. V. Pikhitsa, H. Jiang, D. P. Brown, A. V. Krasheninnikov, A. S. Anisimov, P. Queipo, A. Moisala, D. Gonzalez, G. Lientschnig, A. Hassanien, S. D. Shandakov, G. Lolli, D. E. Resasco, M. Choi, D. Tomanek, E. I. Kauppinen, *Nat. Nanotechnol.*, 2007, **2**, 156.
23. S. Sridhar, C. Tiwary, S. Vinod, J. J. Taha-Tijerina, S. Sridhar, K. Kalaga, B. Sirota, A. H. C. Hart, S. Ozden, R. K. Sinha, Harsh, R. Vajtai, W. Choi, K. Kordás, P. M. Ajayan, *ACS Nano*, 2014, **8**, 7763.
24. J. T. Li, W. Lei, X. B. Zhang, X. D. Zhou, Q. L. Wang, Y. N. Zhang, B. P. Wang, *Appl. Surf. Sci.*, 2003, **220**, 96.
25. Y. L. Wu, Y. N. Li, P. Liu, S. Gardner, B. S. Ong, *Chem. Mater.*, 2006, **18**, 4627.
26. J. E. Jung, Y. W. Jin, J. H. Choi, Y. J. Park, T. Y. Ko, D. S. Chung, J. W. Kim, J. E. Jang, S. N. Cha, W. K. Yi, S. H. Cho, M. J. Yoon, C. G. Lee, J. H. You, N. S. Lee, J. B. Yoo, *Phys. B* 2002, **323**, 71.

27. M. Pudas, J. Hagberg, S. Leppavuori, IEEE Trans. Electron. Packag. Manufact., 2002, **25**, 335.
28. J. J. Schneider, J. Engstler, S. Franzka, K. Hofmann, B. Albert, J. Ensling, P. Gutlich, P. Hildebrandt, S. Dopner, W. Pfleging, B. Gunther, G. Muller, Chem. Eur. J., 2001, **7**, 2888.
29. S. B. Rane, T. Seth, G. J. Phatak, D. P. Amalnerkar, M. Ghatpande, J. Mater. Sci., 2004, **15**, 103.
30. C. Ballif, D. M. Huljić, G. Willeke, A. Hessler-Wyser, Appl. Phys. Lett., 2003, **82**, 1878.

Graphical and textual abstract for manuscript “Facile synthesis of nanostructured carbon materials over Raney nickel catalyst films printed on Al_2O_3 and SiO_2 substrates” by Jih-Fong Lin et al



Films of porous Raney nickel catalyst particles deposited on various substrates by stencil printing from dispersions of the catalyst and poly(methyl methacrylate) in 2-(2-butoxyethoxy)ethyl acetate offer a facile platform for synthesizing nanostructured carbon-nickel composites for direct use as electrodes in electrochemical applications as well as in field emitter devices.